Carbon Capture Science & Technology 13 (2024) 100256

Contents lists available at ScienceDirect

Carbon Capture Science & Technology

journal homepage: www.elsevier.com/locate/ccst

Full Length Article

Potential of carbon dioxide spraying on the properties of 3D concrete printed structures

Yi Wei Daniel Tay[a], Sean Gip Lim[a], Bandar A. Fadhel[b], Issam T. Amr[b], Rami A. Bamagain[b], Ali S. Al-Hunaidy[b], Suvash Chandra Paul[a,*], Ming Jen Tan[a]

[a] Singapore Centre for 3D Printing, School of Mechanical & Aerospace Engineering, Nanyang Technological University, 50 Nanyang Avenue 639798, Singapore
[b] Carbon Management Division, Research & Development Center, Saudi Aramco, Dhahran 31311, Saudi Arabia

ARTICLE INFO

Keywords:
Carbon capture and sequestration
Carbon neutrality
Climate change mitigation
3D concrete printing
Sustainable construction

ABSTRACT

Achieving net carbon neutrality is a global goal toward mitigating climate change presumed consequences. The building and construction sector, responsible for approximately 40 % of greenhouse gas emissions, requires innovative zero-carbon technologies. This paper investigates the synergistic potential of combining 3D concrete printing (3DCP) and carbon capture and sequestration (CCS) to advance net carbon neutrality in construction. By implementing different CO2 spraying regimes, this study demonstrates improved carbon dioxide (CO_2) uptake and the crystallinity of precipitated calcium carbonate ($CaCO_3$). The findings indicate that the method's effectiveness heavily relies on appropriate printing parameters and curing conditions. Chamber-cured samples exhibit the highest CO_2 uptake but the lowest mechanical strength, while ambient-cured samples show the opposite trend. It is also important to note that the duration of CO_2 exposure in this study was relatively short, resulting in limitations in both CO_2 uptake and strength gain. Nevertheless, this study highlights the potential of synergistically combining 3DCP and CCS technologies for net carbon neutrality, emphasizing the critical role of the construction sector in achieving global emission reduction targets.

1. Introduction

The recent covid-19 pandemic has led to significant disruptions in the building and construction industry, exacerbating prevalent challenges such as labor shortages, supply chain restrictions, and increased costs (Alsharef et al., 2021; Gara et al., 2022). The application of concrete formworks, despite being a ubiquitous method of construction, remains a significant contributor to some of these issues. Formwork accounts for about 10 % of total building expenditure, 40–60 % of concrete framework costs, and nearly 20–30 % of construction waste (Shin et al., 2012; Cheng et al., 2022). Moreover, almost 40 % of energy-related carbon dioxide (CO_2) emissions and 36 % of final energy consumption worldwide can be attributed to building and construction activities (Xue et al., 2022). The production of ordinary Portland cement (OPC) alone, which is a primary binding agent of concrete, is responsible for 5–8 % of total greenhouse gas (GHG) emissions (Sousa and Bogas, 2021). Despite reductions in emissions during the pandemic, global CO_2 levels remain high, posing significant climate risks (Hao and Chen, 2023). In this context, 3D concrete printing (3DCP) has emerged as a promising, sustainable alternative to traditional construction methods, leveraging automation to deliver efficient construction (Tay et al., 2023).

A widely adopted strategy to minimize the carbon footprint of concrete is to partially or completely substitute ordinary Portland cement (OPC) with more sustainable alternatives, such as supplementary cementitious materials (SCMs) used in alkali-activated geopolymer concrete (Panda et al., 2017; Amran et al., 2020). Examples of SCMs include industrial by-products like silica fume, fly ash, and slag, which can offer comparable or even enhanced durability and strength relative to traditional concrete. For example, Panda et al. (2017) developed a 3D-printed geopolymer material that is well-suited for large-scale, extrusion-based printing systems.

Besides the formulation of mix designs with a lower associated carbon footprint, another approach to reduce emissions in construction involves curing of concrete with captured CO_2, a technique also known as accelerated carbonation curing (ACC) (Ahmad et al., 2017). When the alkaline constituents of concrete, such as portlandite (CH) and calcium silicate hydrates (C-S-H), react with CO_2 gas, it induces the precipitation of calcium carbonate ($CaCO_3$) minerals (Zajac et al., 2022). This process, known as carbon mineralization, is a key principle that governs the permanent sequestration of CO_2 in concrete materials. Existing studies conducted by Douba et al. (2022), demonstrate that 3D printing using carbon-cured mixtures containing magnesium oxide (MgO) cement re-

* Corresponding author.
E-mail address: suvash.cp@ntu.edu.sg (S.C. Paul).

https://doi.org/10.1016/j.ccst.2024.100256
Received 31 May 2024; Received in revised form 4 July 2024; Accepted 19 July 2024

sults in substantial improvements in the compressive strength of printed specimens compared to their conventionally cast counterparts. The enhanced strength was attributed to a higher CO_2 intake, correlated to a larger exposed surface area with corresponding infill patterns. A higher rate of water evaporation, often exacerbated by a lack of protective casing, was also noted to increase the porosity of samples, potentially enabling more carbonation reactions to occur.

Incorporating carbonated aggregates in the mixture can improve the compressive strength (Sun et al., 2022). Sun et al. (2022) shows that the incorporation of carbonated recycled fine aggregates (CRFA) increase the 28-day compressive strength of the 3D printed mortars by up to 68.5 % when 100 % natural fine aggregates (NFA) were replaced with CRFA, compared to untreated recycled fine aggregates (RFA). Additionally, the enhancement of carbonation efficiency was described as achievable by reducing printed filament widths and increase in CO_2 curing durations, as shown in existing literature (Wang et al., 2023). Wang et al. (2023) found that there was up to 24 % increase in carbonation with printed samples of 10 mm filament width after 24 h carbonation, alongside improvements in mechanical properties such as compressive strength, splitting tensile strength, and interlayer bonding strength. Carbonation depths along the interlayer position of 3DCP samples were also observed to be higher than those within the filaments, especially during early ages of CO_2 curing.

Corresponding to the aforementioned literature, methods to achieve carbon sequestration in cementitious products generally involve subjecting aggregate prior mixing or postprocessing concrete to chamber curing at elevated temperature, pressure, humidity, and concentrated CO_2 parameters (Sun et al., 2022; Wang et al., 2023; Dixit et al., 2021; Kim et al., 2021). Further measures to accelerate the carbonation of concrete may include spraying CO_2 during its mixing phase (Monkman et al., 2016; He et al., 2017; Qian et al., 2018). The combination of both carbonation mixing and curing processes was stated to achieve a 10 % CO_2 uptake in paste samples, an over 30 % increment as compared to curing-only treatments (He et al., 2017). Nevertheless, despite positive claims reported in some of these articles, the authors expressed concern that accelerated carbonation methods via chamber curing can be time- and energy-consuming, potentially limiting their compatibility with automated technologies like 3DCP. Monte Carlo simulations by Ravikumar et al. (2021) using published experimental datasets projected that CO_2 utilization in concrete curing or mixing has a higher probability of producing a net increase in CO_2 footprints instead.

To automate the CCS technology and incorporating it with 3DCP, this research will investigate the potential and effects of sequestering CO_2 into 3D printable concrete via direct spraying of pressurized CO_2 gas and steam across surfaces of each filament layer using a custom-built gantry printhead set-up. This work is inspired by an existing patent (Al-Khowaiter et al., 2021). Various configurations of the experimental setup will be analyzed to evaluate its effectiveness in promoting the carbon sequestration of cement-based material during its printing phase. Samples extracted from the bulk of printed concrete filaments will be subjected to thermogravimetric analysis (TGA) to characterize the quantity of stable carbonates precipitated after a 28-day curing period, corresponding to the degree of carbon uptake in samples with respect to their associated print configuration. To the best of the authors' knowledge, there is a lack of studies conducted to investigate the impacts of integrating CCS technologies with 3DCP. Therefore, the purpose of this study aims to serve as an initiative for further exploration and research in this domain.

2. Experimental program

2.1. Material preparation and curing conditions

The raw material used in the study were ordinary Portland cement (OPC, ASTM Type 1), silica Fume (Undensified, Elkem), superplasticiser and river sand. The same mix design is used for all prints. For consistency in the experiments, all concrete admixtures were mixed according to the same guidelines. First, all powder elements (i.e., aggregates and cementitious powder) were dry mixed at low speeds using a force action mixer (SoRoTo 80 L mixer) for 3 min before hydrating solutions such as water and superplasticizers were gradually added. This process ensure even dispersion and distribution of solid particles/powder, after which 10 minutes of high-speed mixing was carried out until homogeneity of the mixture was achieved. Information on the percentage raw materials used in this study cannot be disclosed due to a non-disclosure agreement with the collaborators.

Table 1
Sample abbreviations.

Abbreviation	Description
CTRL	Control sample printed without steam and CO_2 spraying which serves as a benchmark for comparison with other samples
CS	Samples printed with steam and single directional CO_2 spraying
DCS	Samples printed with steam and dual directional CO_2 spraying

All samples were covered with clear plastic for four hours immediately after printing. Following this initial period, the samples underwent one of two curing regimes: ambient curing or chamber curing. For the ambient-cured samples, they were wrapped in clear plastic after the initial four hours to prevent moisture loss due to evaporation. These samples were then cured under laboratory conditions at 22.5 °C and 61 % relative humidity (RH) for 28 days. For the chamber-cured samples, the plastics were removed and were placed in a curing chamber (Memmert, CTC 256) after the initial four hours. These samples were cured at 60 °C and 95 % RH for 28 days. In this study, different abbreviations were assigned to the different printing processes investigated to simplify the naming of samples (See Table 1).

2.2. Printing parameters

A three-axis gantry printer (Mitsubishi customed-made concrete printer) and a progressive cavity pump (MAI, Lyra) were utilized as the printing setup. The material was transported from the material reservoir to the square nozzle with an orifice size of 20 mm by 20 mm through a three-meter, one-inch hose. The gantry's printing speed remained constant at 100 mm/s for all mixtures and has a material flow rate of 39 ml/s. All samples were prepared using the same printing parameters as mentioned. The control sample (CTRL) was prepared without steam and CO_2 spraying during the printing process. This ensured that any differences observed were due to the steam and CO_2 addition during printing and not variations in any other printing parameters. Fig. 1(a) showcases the printed samples used for various testing. After the printing process, the printed blocks created using the print path depicted in Fig. 1(b) were cut into smaller sections, measuring 50 mm in length for the compressive strength test and 1 mm for the TGA test, using a diamond cutter (Struers, Secotom-60). Fig. 1(c) illustrates the schematic diagram of the print path for the samples employed in the TGA and compressive strength tests.

All specimens have a solidity ratio (SR) in the range of 0.95 to 1.05. SR can be used to determine the consistency of the printed filament based on the printing parameters (Tay et al., 2019). Two different printing parameters can have the same SR which means the amount of material deposited per unit length is the same. SR is defined by Eq. (1).

$$SR = {}^{1000Q}/_{A_n \times V_n} \tag{1}$$

where A_n is the area of the nozzle orifice, V_n is travel speed and Q is the flow rate of the material.

2.3. Single directional CO_2 spraying with steam (CS)

In an effort to enhance CO_2 uptake, a direct spraying approach was employed by positioning a dedicated CO_2 nozzle alongside the concrete

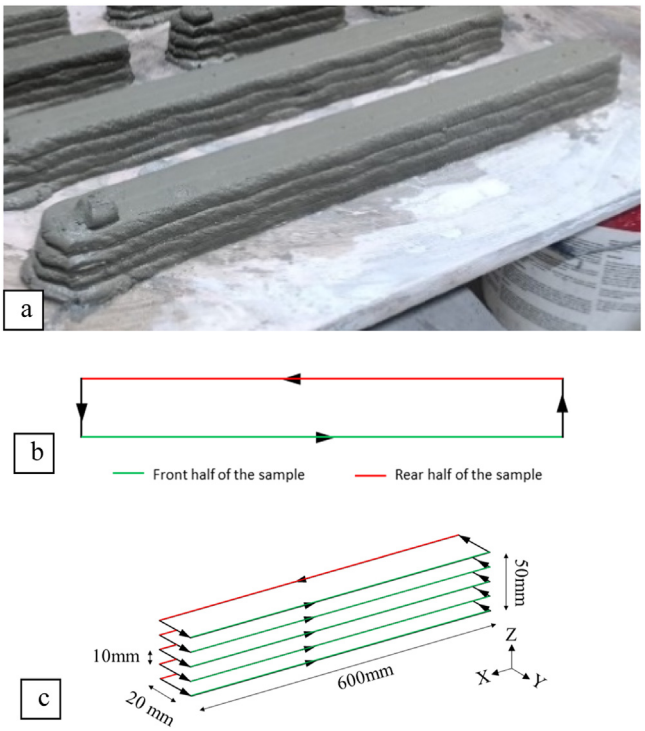

Fig. 1. (a) 3D printed samples for TGA and mechanical analysis; (b) Top view of the printing path to differentiate the front and rear half of the sample; (c) Schematic diagram for the print path with dimensions for compressive strength and TGA test.

nozzle during the printing process. The carbon dioxide gas (Air Liquide, ALPHAGAZ ONE) utilized in this research possesses a high purity level of 99.998 %. The use of high purity gases, as reported in existing literature (Ashraf et al., 2016; Tu et al., 2016; Mo and Panesar, 2012; Fernández-Carrasco et al., 2008), maximizes the quality and reliability of our analysis. Fig. 2 illustrates the setup, wherein the outlet of the CO_2 nozzle is strategically positioned directly above the concrete filament. This configuration allows for the spraying of CO_2 into the filament, facilitating the sequestration of carbon dioxide as the concrete is being printed.

Due to the close proximity of the nozzle and the substantial flow of CO_2 directed onto the top surface of the filament, a challenge arises in terms of material displacement. Some of the material from the filament tended to be blown off as a result. To address this issue, the pressure from the CO_2 gas cylinder was maintained at a fixed value of 3 bar. This pressure setting was carefully determined to strike a balance between ensuring an optimal amount of CO_2 penetration into the cementitious filament during printing and preventing excessive displacement of the filament caused by the CO_2 nozzle outlet pressure.

Steam was introduced in this study to increase the temperature and moisture. It was presented by Zhan et al. (2016) and Zeyad et al. (2022) that the moisture content and increased temperature greatly influence the CO_2 curing degree and significantly improve strength gain.

Fig. 2 provides a schematic diagram depicting the side view of the printing setup featuring a single CO_2 nozzle with a steam nozzle, illustrating its attachment and its role in printing the front and rear halves of the sample. Due to this setup, there is a distinction in the application of CO_2 on the filament's surface. For the front half of the sample, CO_2 is applied to the bottom of each layer, while for the rear half of the sample, CO_2 is directed onto the top surface of the filament.

In pursuit of improving CO_2 uptake, previous investigations have revealed that the introduction of steam can yield favorable results (Kim et al., 2021). The presence of elevated temperature and higher humidity levels has demonstrated the potential to enhance CO_2 uptake in cementitious samples. In this study, the temperature of the steamer was fixed at 100°C, while the outlet of the steamer was set at a flow rate of 35 ml/min.

2.4. Dual directional CO_2 spraying with steam (DCS)

In section 2.2.1, it was discussed that due to the fixed position of the gas attachment, CO_2 infusion into the concrete samples will differ between the front and rear halves of the filament. To address this issue and achieve consistent CO_2 spraying on both sides of the sample, a dual nozzle setup was implemented. This involved placing pneumatic tubes on both sides of the nozzle, with the hypothesis that it could increase CO_2 uptake and ensure uniform distribution throughout the entire sample.

Similar to the CS method, steam is introduced to increase the temperature and moisture. The spraying of CO_2 for the CS method is shown in Fig. 3. The CO_2 gas is discharged in the opposite direction of the nozzle movement, which ensures that CO_2 is being blown onto the top surface of the printing filament as shown in Fig. 4. By implementing two distinct spray directions, the aim is to ensure a uniform application of CO_2 onto the filament's upper surface and to reduce delamination. This is with the intention of effectively incorporating the CO_2, as depicted in Fig. 4.

2.5. Thermogravimetric analysis (TGA)

The TGA is carried out using a thermogravimetric analyser (TA Instruments TGA-Q500) by quantifying the estimated degree of CO_2 uptake in the concrete samples by its mass loss percentage. The mass of the specimens to be placed in the equipment must weigh between 10 mg - 20 mg. To obtain samples for analysis, the concrete specimens were sliced into thin sheets before pulverizing them into fine powders, to capture the entire distribution of carbonation depths throughout its cross-section.

The test specimens will be heated over a range of temperature from 20°C to 950°C at a constant rate of 20°C/min in a nitrogen atmosphere. The presence, phase, and quantity of stable carbonates (i.e., $CaCO_3$) precipitated in each sample is determined by its mass loss percentage across a temperature range from 520°C to 950°C, and the CO_2 uptake

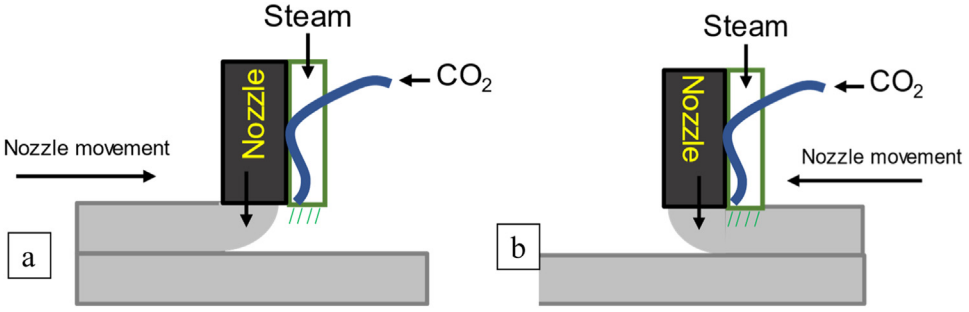

Fig. 2. Schematic diagram on the side view of printing with concrete and CO_2 spraying nozzle for the (a) front half of sample (b) rear half of sample.

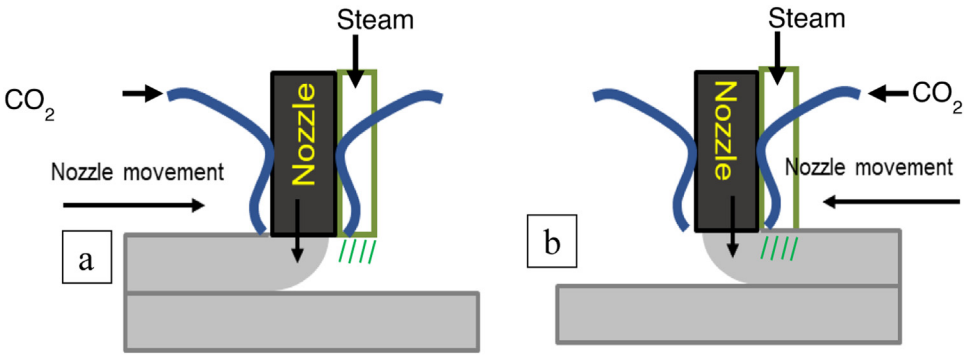

Fig. 3. CO_2 dual directional printing for second approach (a) front half of sample (b) rear half of sample.

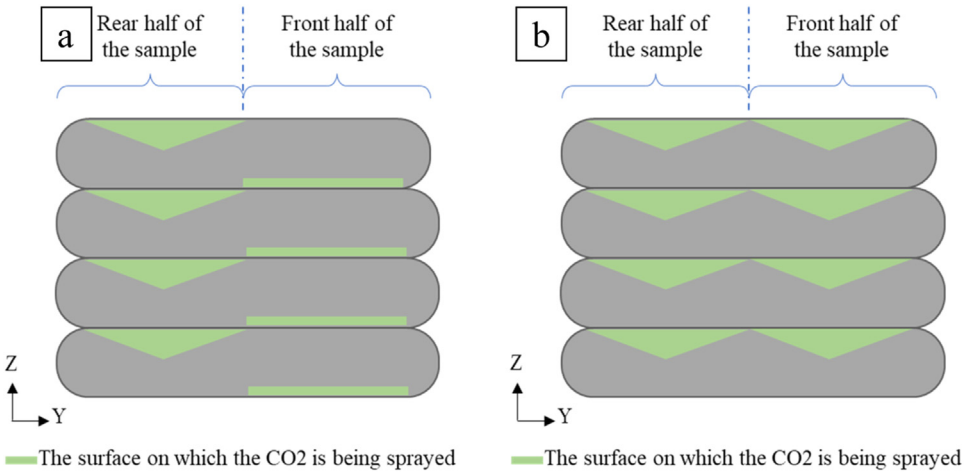

Fig. 4. Schematic drawing of the sample cross-section for (a) CS and (b) DCS samples. Regions highlighted in green represent where CO_2 and steam sprays were introduced during printing.

can be calculated using Eqs. (2) to (4) (Tu et al., 2016):

$$\%m_{CaCO_3,DC} \approx \frac{m_{520°C} - m_{720°C}}{m_{20°C}} \times 100\% \quad (2)$$

$$\%m_{CaCO_3,HC} \approx \frac{m_{720°C} - m_{950°C}}{m_{20°C}} \times 100\% \quad (3)$$

$$\%m_{CaCO_3,Net} = \%m_{CaCO_3,DC} + \%m_{CaCO_3,HC} \quad (4)$$

where, $\%m_{CaCO_3,DC}$ is the percentage mass loss of the poorly crystallized $CaCO_3$, $\%m_{CaCO_3,HC}$ is the percentage mass loss of the highly crystallized $CaCO_3$ and $\%m_{CaCO_3,Net}$ is the net percentage mass loss of crystallized $CaCO_3$.

2.6. Mechanical strength testing

The compression load test was conducted on ALFA compression tester. The investigation of the effect of carbonation on the mechanical strength of 3D printed concrete was conducted after a curing period of 28 days. The purpose of this test was to determine the strength characteristics of the samples under various printing and curing conditions and compare them to the control sample. The mechanical strength assessment serves as a crucial indicator of the performance and structural integrity of the 3D printed concrete. By subjecting the cured samples to rigorous testing, valuable insights can be gained regarding the influence of different printing and curing parameters on the material's strength properties. Previous literature has demonstrated a potential increase in strength when CO_2 is employed for curing (Kim et al., 2021). This phenomenon can be attributed to the reduction in pore size resulting from the carbonation curing process (Kim et al., 2021). To ensure standardized and reliable testing, the procedure for assessing the mechanical strength of the samples adhered to the guidelines outlined in ASTM standard C109 (ASTM C109 /C109M-21 2021). The printed samples for compressive test were cut into 50 mm length cubes using a diamond cutter (Secotom-60, Struers) and was tested only in the Z-direction.

2.7. Macroscopic characterization

The investigation of the macroscopic morphology of the specimens involved an analysis of the fractured surfaces resulting from slicing the cross section of the sample. To capture detailed images of the sample surfaces, a high-resolution 12-megapixel camera was employed. These images were crucial for facilitating an in-depth analysis of the cross-sections of the specimens.

Examining and identifying subsurface voids and interlayer delamination caused by the direct spraying of CO_2 and steam onto the surfaces of the extruded printable mortar can give a deeper understanding of the impact of the printing process on the formation and distribution of voids. This information was crucial for understanding the potential structural weaknesses and defects that may arise from the printing process. Subsurface voids refer to empty spaces or cavities located beneath the surface of the specimen, while interlayer delamination occurs when layers of the printed mortar separate from each other.

2.8. Permeable voids test

The permeable voids test was carried out in accordance with ASTM standard C642 (ASTM C642-21 2021) to determine the physical characteristic of the concrete material, such as permeable pore structure, using very limited equipment. The results were compared to it mechanical strength and macroscopic appearance for verification.

3. Results and discussion

3.1. Thermogravimetric analysis

When calcium silicates in cement interact with water, they form calcium hydroxide ($Ca(OH)_2$) and calcium silicate hydrates (C-S-H) in an exothermic reaction (Kim et al., 2013). C-S-H is crucial for the durability and strength of cement and concrete (Madadi and Wei, Jan. 2022). Exposure of CO_2 with $Ca(OH)_2$ and C-S-H will transform to $CaCO_3$ (Haghnegahdar et al., 2011). When $CaCO_3$ is exposed to high temperatures, the material breaks down to calcium oxide and CO_2 (Rodríguez et al., Sep. 2008). In the TG result, the mass loss observed between 520 °C and 950 °C correlates with the amount of CO_2 in the sample (Villain et al., 2007). This decomposition profile is used to evaluate the efficacy of CO_2 jetting in CO_2 sequestration.

$CaCO_3$ formation can fill *meso* and micro pores, thereby enhancing the material's microstructure (Mehdizadeh et al., 2021). Several factors, including cement's chemical composition, impurities, and additives, can influence the crystallinity of $CaCO_3$ (Chang et al., 2017). Crystallinity is categorized as poorly crystalline between 520 °C to 720 °C and well-crystalline between 720 °C to 950 °C (Tu et al., 2016; Vogler et al., 2022). Literature supports that poorly crystalline values are typically higher than well-crystalline values due to the nature of the crystallization process (Tu et al., 2016). When $CaCO_3$ forms in a cementitious matrix, it often starts in a disordered, poorly crystalline state, especially in the initial stages, due to environmental conditions favoring rapid nucleation and growth. Poorly crystalline forms are less stable and more reactive compared to well-crystalline $CaCO_3$, making them more prevalent in certain conditions.

Figs. 5–7 illustrate the thermogravimetry (TG) and derivative thermogravimetry (DTG) curves, the percentage weight content of poorly and well-crystalline $CaCO_3$, and the percentage weight content of total precipitated $CaCO_3$ in samples, respectively. In general, the total quantity of $CaCO_3$ precipitated in chamber cured samples was relatively consistent. The chamber-cured CTRL samples had approximately 25 % higher CO_2 uptake than their ambient-cured counterpart, which may be attributed to the acceleration of both hydration and carbonation reactions due to increased temperature and humidity levels during curing (Liu et al., 2020). A significant portion of CO_2 sequestered in all chamber-cured samples, however, stemmed from the precipitation of poorly crystalline $CaCO_3$ (See Fig. 6), while ambient-cured samples showed a higher percentage sample weight of well-crystalline $CaCO_3$. The results algin well with existing literature (López-Arce et al., 2011; Steiner et al., 2020). López-Arce et al. (2011) shows that high relative humidity conditions would enhance the formation of $CaCO_3$ polymorphs, such as aragonite and calcite, that possess enhanced thermodynamic stability over carbonation products of samples cured under a relatively lower RH. Steiner et al. (2020) explained that this could be due to an increased presence of free water, which enables water monolayers to form water films along particle surfaces of the prepared sample, promoting the nucleation of $CaCO_3$ across these aqueous layers. However, the increase in early-age temperature exposure may have contributed to poorer crystallinity of $CaCO_3$ phases.

The crystallinity and percentage content of $CaCO_3$ in samples is significantly dependant on its manufacturing methods and curing approach. As observed in Fig. 6, the poorly crystalline phases of $CaCO_3$ increase following the incorporation of CO_2 and steam sprays, with ambient cured samples observed to increase more extensively than chamber cured samples. The differences between the total CO_2 sequestered in ambient-cured and chamber-cured samples noticeably reduces with the integration of CO_2 and steam spraying methods during 3DCP, particularly for DCS samples. The ambient-cured DCS samples had approximately 24 % more $CaCO_3$ by weight than the ambient-cured control samples and nearly matched the best results of the chamber-cured samples. Moreover, much of the improvements in CO_2 sequestered for DCS ambient samples were attributed to the mineralization of well-crystalline $CaCO_3$ phases. The higher stability of carbonates in ambient-cured DCS samples suggests that these samples perform better than chamber-cured ones, even though both types produce nearly the same amount of $CaCO_3$. Overall, DCS samples performed the best, with ambient-cured samples showing results comparable to those of chamber-cured ones. This suggests that ambient curing could be a viable alternative to chamber curing, potentially improving the hydration kinetics and carbonation of concrete.

For net CO_2 uptake as shown in Fig. 7, CS samples had the highest standard deviation among all samples, indicating instability in sequestration performance. As described and illustrated in Section 2.2, CO_2 spraying onto CS samples were at closer proximity to upper layers of samples during the rear printing direction. This resulted in slight dispersal of the material from freshly deposited filament surfaces, causing the formation of larger gaps and cavities along its inter-layers. On the contrary, DCS samples had CO_2 sprayed from a greater distance away from the bottom surfaces of the extruded material, resulting in less distortion at the filament inter-layers. The formation of gaps and cavities following material dispersion from the filament surfaces may have contributed to the instability of sequestration performance of CS samples. This shows that better control over the direction of steam relative to CO_2 spraying and 3D concrete printing will be crucial to achieve stable and consistent result in carbon sequestration.

The formation of well-crystallized $CaCO_3$ is crucial for the long-term performance and CO2 sequestration capacity of concrete. Based on our findings and existing literature, several strategies can be employed to increase the proportion of well-crystallized $CaCO_3$. Our results demonstrated that ambient-cured samples exhibited a higher percentage of well-crystalline $CaCO_3$ compared to chamber-cured samples, suggesting that lower temperature and humidity conditions during curing may promote the formation of more stable, well-crystallized CaCO3. This observation aligns with the work of Lopez-Arce et al. (Steiner et al., 2020), who showed that moderating relative humidity during curing can enhance the formation of more stable $CaCO_3$ polymorphs like aragonite and calcite.

The controlled CO_2 exposure method, particularly the DCS approach in ambient-cured samples, showed improvements in well-crystalline $CaCO_3$ formation. This finding is consistent with research by Xian and Shao (2021), who demonstrated that ambient pressure performed better than high pressure in reducing pore volume and refining capillary pore size. While not directly examined in this study, allowing for longer curing periods could potentially increase the proportion of well-crystallized $CaCO_3$. The formation of strong crystalline $CaCO_3$ was due to the carbonation of phases, such as calcium hydroxide (CH), C-S-H and calcium silicates (Rostami et al., 2012) suggesting that extended CO_2 exposure time might yield better results.

These findings collectively suggest multiple avenues for optimizing the formation of well-crystallized calcium carbonate in concrete. However, it is important to note that the interplay between these factors in the context of 3D printed concrete may be complex. Further research focusing specifically on these aspects in 3D printed concrete would be beneficial for optimizing CO_2 sequestration and concrete performance. Such studies could provide valuable insights into the most effective combinations of curing conditions, CO_2 exposure methods, and material compositions for maximizing the proportion of well-crystallized CaCO3 in 3D printed concrete structures.

3.2. Mechanical strength

The samples cured in chambers consistently showed lower compressive strength compared to those cured in ambient conditions. The addition of CO_2 and steam sprays in these chamber-cured samples did not significantly improve strength as shown in Fig. 8. The CS and DCS chamber-cured samples exhibited a slight to negligible decrease in compressive strength, when compared to the CTRL samples. On the contrary, the introduction of CO_2 and steam was found to enhance the compres-

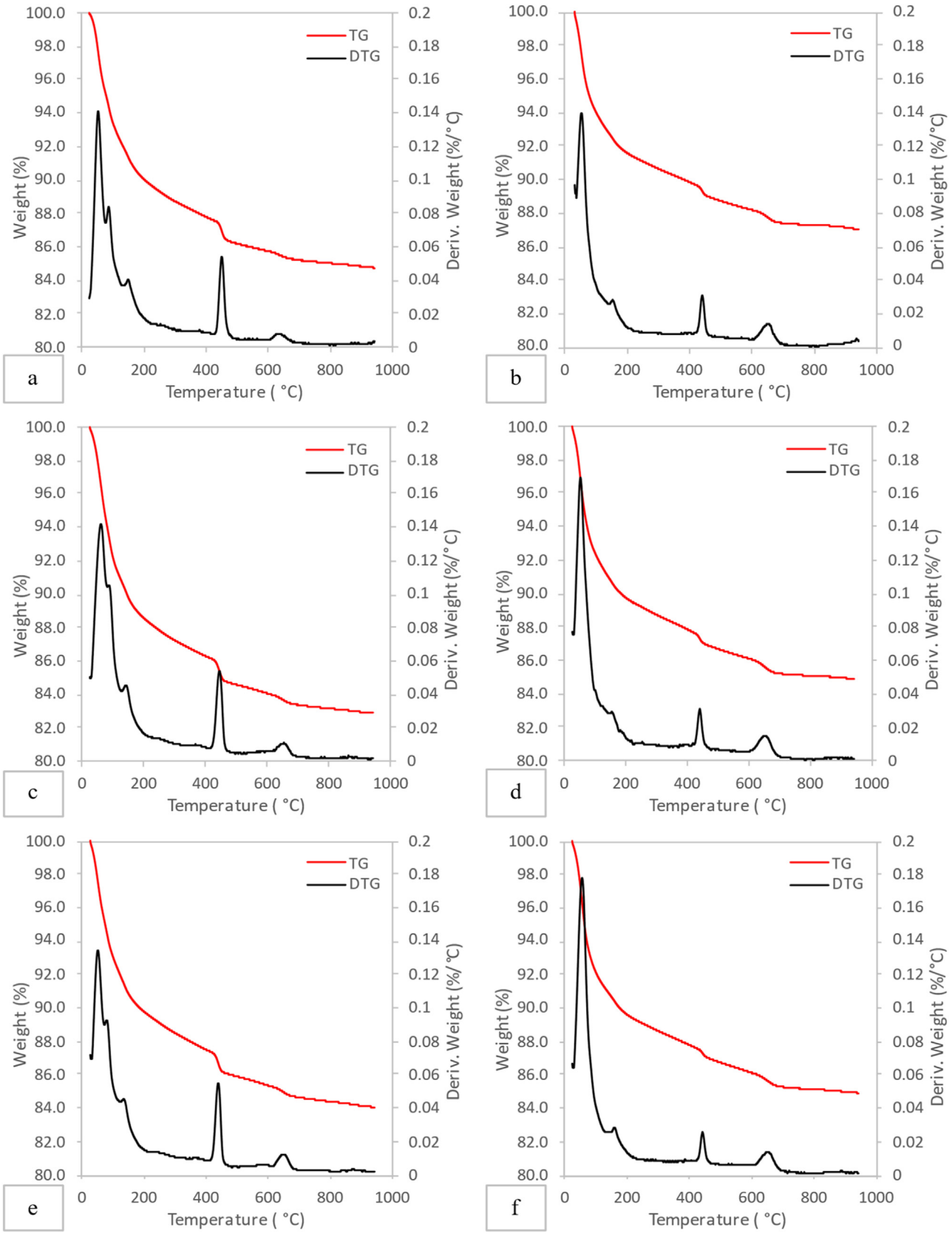

Fig. 5. Thermogravimetry and derivative thermogravimetry (TG-DTG) curves for the control (CTRL), single direction (CS) and dual direction samples (DCS) with chamber (C) and ambient (A) curing (a) CTRL_A, (b) CTRL_C, (c) CS_A, (d) CS_C, (e) DCS_A, and (f) DCS_C samples.

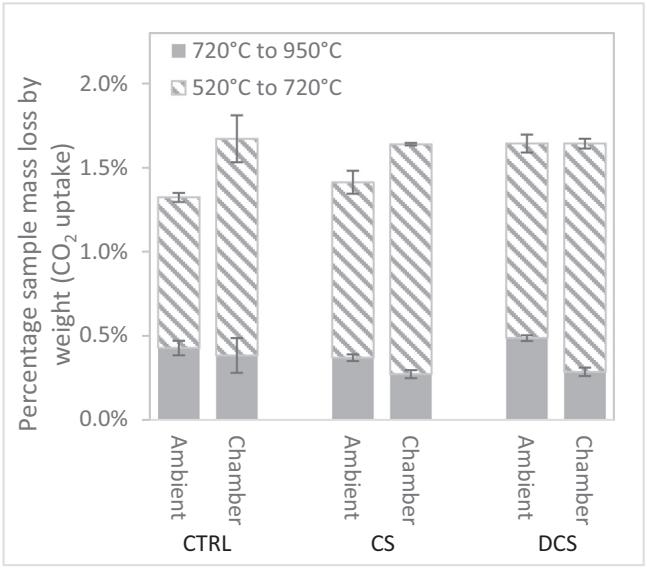

Fig. 6. Percentage sample mass loss for the control (CTRL), single direction (CS) and dual direction samples (DCS) with chamber and ambient curing from 520°C to 720°C and 720°C to 950°C.

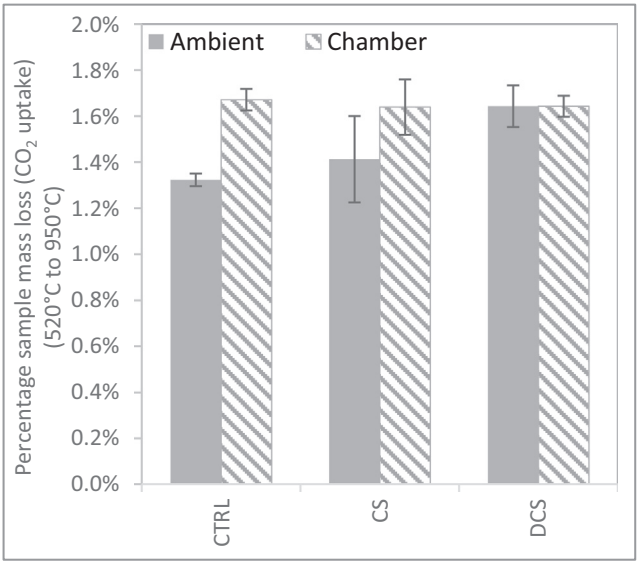

Fig. 7. Percentage Sample Mass Loss from 520°C to 950°C.

sive strength of the ambient cured samples. The CS and DCS ambient-cured samples exhibited an 8.45 % and 15.0 % increase in compressive strength, respectively, compared to the CTRL samples. Despite the earlier discussion of gaps and cavities in filaments in Section 3.1, the printing processes integrated with CO_2 and steam show a more stable and positive improvement in compressive strength results with ambient-cured samples compared to chamber-cured samples.

Tay et al. (2023) reported that spraying only CO_2 to the filament can cause a drying effect, leading to reduced strength. Previous studies have also shown that moisture significantly impacts layer adhesion, potentially improving strength and reducing plastic shrinkage (Moelich et al., 2021; Moelich et al., 2020). Additionally, increase in moisture content can cause lower internal stress within the layers of 3D printed structures (Slavcheva, Feb. 2019). Xiao et al. (2021) mentioned that interlayer bonding strength is directly proportional to the mechanical properties of 3D printed concrete. This suggests that the steam used in this study improved bonding between filaments, thereby enhancing the compressive strength of the concrete. The decrease in mechanical properties due to chamber curing may also be exacerbated by competing interests for ions between pozzolanic reactions and carbonation of the cementitious mixture, compromising the formation of C-S-H gels, which are key to mechanical strength development, as shown in existing literature (Dixit et al., 2021; Justnes et al., 2020).

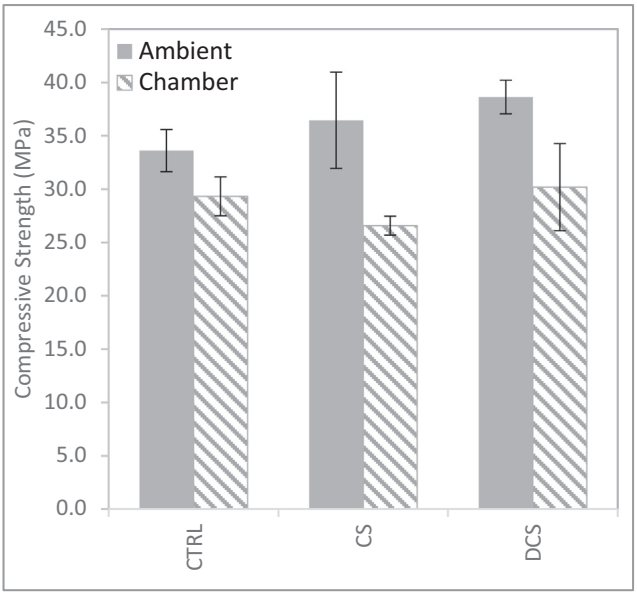

Fig. 8. Compressive strength result for the control (CTRL), single direction (CS) and dual direction samples (DCS) with chamber and ambient curing.

In general, despite the positive influence on CO2 uptake, chamber-cured samples exhibited lower mechanical strength compared to ambient-cured samples. Both the printing and curing methods significantly influence the mechanical properties of all samples, affecting the formation of cavities and moisture along the inter-layers during deposition, which impacts layer bonding.

3.3. Macroscopic morphology

Compared to the CTRL samples, a significant increase in larger voids and interlayer delamination has been observed in the CS and DCS samples. This delamination of the filaments in the CS and DCS samples is attributed to the addition of CO_2 and steam in the process. In contrast, the CTRL sample undergoes continuous extrusion of material from the gantry print head onto the previous layers without interruption (see Fig. 9). Interestingly, chamber-cured samples exhibited significantly greater extents of delamination in terms of both width and length compared to ambient-cured samples. The DCS samples displayed better bonding than the CS specimens, potentially due to the optimized positioning and targeting of CO2 sprays relative to the print path. When analysing the average external dimensions of the sample cross-sections, consistency in height and width measurements was observed. This implies that the introduction of CO_2 and steam sprays during printing had little to no detrimental impacts on the slump characteristics of the freshly deposited mortar. Moreover, the results suggest that the mortar exhibited suitable rheological properties for retaining its overall shape structure, despite experiencing the partial dispersal of filament components during 3DCP when subjected to the localized shearing forces of pressurized CO_2 sprays and steam.

3.4. Permeable voids

The mechanical properties of cementitious materials are significantly influenced by their density and the presence of voids. Concrete with

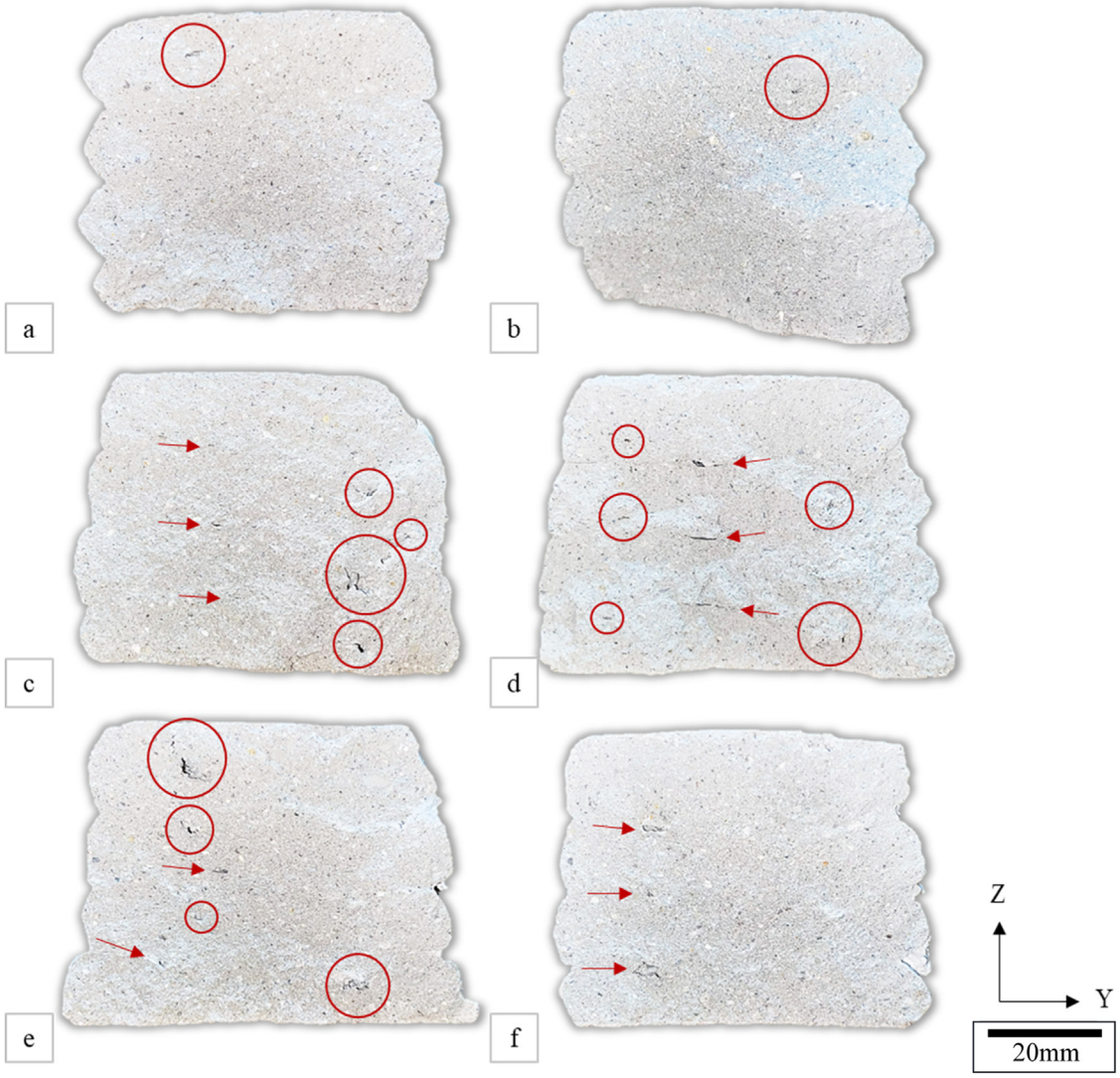

Fig. 9. Cross-section of the specimens for the control (CTRL), single direction (CS) and dual direction samples (DCS) with chamber (C) and ambient (A) curing. (a) CTRL_A, (b) CTRL_C, (c) CS_A, (d) CS_C, (e) DCS_A, and (f) DCS_C. Circled and pointed in red are visually noticeable subsurface voids and interlayer delamination.

higher density tends to exhibit greater strength compared to less dense concrete. The presence of voids compromises the material's load-bearing capacity. Additionally, denser concrete is characterized by reduced permeable voids and lower porosity, contributing to improved durability.

As depicted in Fig. 10, the volume of permeable voids in the concrete samples is an important indicator of their quality. Notably, the chamber samples display a higher amount of permeable voids compared to the ambient samples. This observation aligns with the compressive strength results shown in Fig. 8, where the chamber-cured samples exhibited weaker strength compared to the ambient-cured samples. The volume of permeable voids also correlates with the findings presented in Fig. 9, which revealed that both the CS and DCS samples has significantly more pores compared to the control sample. This difference in porosity is attributed to the steam and CO_2 spraying process employed during printing.

The presence of voids in concrete significantly influences crack propagation and the overall strength of the material. In less dense concrete, cracks have a higher propensity to penetrate easily, primarily following weaker bonds within the material, such as the filament bonds in the case of 3D printing. Under increasing compressive stress, strains orthogonal to the applied loading induce additional cracks, which predominantly propagate through these weak bonds. With continued loading, the number of cracks increases, and they eventually coalesce, leading to material failure (Zaitsev and Wittmann, 1981).

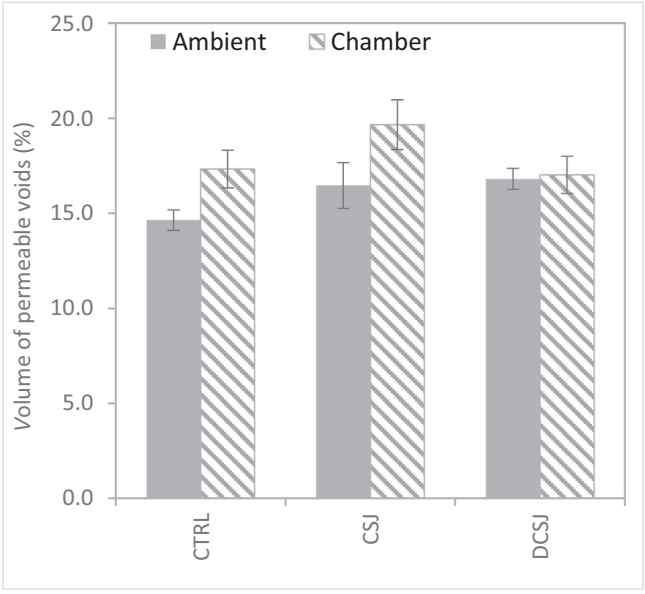

Fig. 10. Volume of permeable voids for the control, single direction (CS) and dual direction samples (DCS) with chamber and ambient curing.

Understanding the relationship between permeable voids and concrete properties is crucial for optimizing the 3D printing process and improving the performance of printed structures. By mitigating the formation of permeable voids and promoting denser concrete, it is possible to enhance the durability, strength, and overall structural integrity of 3D printed components. Moreover, the findings from this study shows the importance of selecting appropriate printing parameters to control the formation of voids and ensure the desired mechanical properties of the printed concrete.

4. Conclusion

In the pursuit of sustainable construction practices, it is crucial to assess the diverse parameters integrating CCS with 3D concrete printing. This understanding plays an important role in devising effective strategies for environmentally responsible construction. This study delves into this precise area, providing valuable insights into the implications of different printing conditions on both the carbonation process and subsequent mechanical properties. These findings hold significance for the seamless integration of CCS techniques within 3D concrete printing for a greener construction industry. The results obtained from the thermogravimetric analysis (TG) and derivative thermogravimetry (DTG) curves, as well as the percentage weight content of poorly and well-crystalline $CaCO_3$, shed light on significant aspects of the carbonation process. It's worth noting that the carbonation process in cementitious materials primarily results in the formation of $CaCO_3$ under the conditions present in this study. This is supported by our thermogravimetric analysis results, which show characteristic decomposition profiles for $CaCO_3$ between 520 °C and 950 °C. Some conclusions drawn are shown below:

- Chamber-cured samples exhibit consistent CaCO3 precipitation, resulting in 25 % higher CO2 uptake than ambient-cured samples. This enhancement may be attributed to elevated temperature and humidity during chamber curing, expediting both hydration and carbonation.
- Chamber-cured samples sequester a significant portion of CO2 as poorly crystalline CaCO3, while ambient-cured samples have a higher percentage of well-crystalline CaCO3. Adoption of the ambient-cured techniques may reduce reliance on chamber curing for large-scale CO2 sequestration in concrete, potentially eliminating geometric constraints for future printable structures.
- CS samples show higher CO2 uptake variability due to specific CO2 application during printing, leading to dispersion and formation of gaps and cavities. These voids negatively affect density and structural integrity, potentially compromising the mechanical properties of concrete. CS ambient-cured samples exhibits an 8.45 % increase in compressive strength, while CS chamber-cured samples experiences a 9.38 % reduction.
- DCS ambient-cured samples achieve higher well-crystalline CaCO3 and have the highest mechanical properties, showing a 15.0 % increase in compressive strength compared to the CTRL.
- The observed improvement in compressive strength for ambient-cured samples using the proposed method can be considered a significant advantage for commercial applications.

Looking ahead, future research can focus on further reducing the carbon footprint of 3D printable concrete while optimizing the dynamics of CO_2 introduction to enhance mechanical properties. Based on the result in this study, there are several parameters that can be improved or altered to improve the CO_2 uptake. Increasing the exposure time by reducing the nozzle size, which in turn increase the print path length, can increase the exposure time. Additionally, 3DCP structures can be constructed hollow with a lattice-designed cross-section, its net area of surfaces exposed to CO_2 will inherently be larger than those of solid cast concrete. Furthermore, changes to its print parameters (e.g., layer height and stand-off distance) can also allow for further adjustments towards the material's degree of compaction and porosity, which are fundamental to CO_2 ingress and mineralization objectives. Following this line of reasoning, the capacity to alter these parameters while simultaneously introducing CO_2 may hence be a more efficient and complementary approach to 3DCP.

Declaration of competing interest

The authors declare that they have no known competing financial interests or personal relationships that could have appeared to influence the work reported in this paper.

CRediT authorship contribution statement

Yi Wei Daniel Tay: Writing – original draft, Writing – review & editing, Conceptualization, Methodology, Investigation, Data curation. **Sean Gip Lim:** Writing – original draft, Writing – review & editing, Conceptualization, Methodology, Investigation, Data curation. **Bandar A. Fadhel:** Writing – review & editing, Resources, Supervision. **Issam T. Amr:** Writing – review & editing, Resources, Supervision. **Rami A. Bamagain:** Writing – review & editing. **Ali S. Al-Hunaidy:** Writing – review & editing. **Suvash Chandra Paul:** Writing – review & editing. **Ming Jen Tan:** Writing – review & editing, Resources, Supervision.

Acknowledgements

This research is supported by Saudi Aramco Technologies Company, and National Research Foundation, Prime Minister's Office, Singapore under its Medium-Sized Centre funding scheme for the Singapore Centre for 3D Printing.

References

Ahmad, S., Assaggaf, R.A., Maslehuddin, M., Al-Amoudi, O.S.B., Adekunle, S.K., Ali, S.I., 2017. Effects of carbonation pressure and duration on strength evolution of concrete subjected to accelerated carbonation curing. Constr. Build. Mater. 136, 565–573. doi:10.1016/j.conbuildmat.2017.01.069.

Al-Khowaiter, A.O., Jamal, A., Amr, I.T., Bamagain, R., Al-Hunaidy, A.S., Fadhel, B.A., 2021. Cementitious Print Head, 3D Printing Architecture, and Cementitious Printing Methodology Patent No. 11236517[Online]. Available:. https://patents.justia.com/patent/20210189745.

Alsharef, A., Banerjee, S., Uddin, S.M.J., Albert, A., Jaselskis, E., 2021. Early impacts of the COVID-19 pandemic on the United States construction industry. Int. J. Environ. Res. Public Health 18 (4). doi:10.3390/ijerph18041559.

Amran, Y.H.M., Alyousef, R., Alabduljabbar, H., El-Zeadani, M., 2020. Clean production and properties of geopolymer concrete; a review. J. Clean. Prod. 251, 119679. doi:10.1016/j.jclepro.2019.119679.

Ashraf, W., Olek, J., Tian, N., 2016. Multiscale characterization of carbonated wollastonite paste and application of homogenization schemes to predict its effective elastic modulus. Cem. Concr. Compos. 72, 284–298. doi:10.1016/j.cemconcomp.2016.05.023.

ASTM C109 /C109M-21, 2021. Standard Test Method for Compressive Strength of Hydraulic Cement Mortars (using 2-in. or [50-mm] Cube Specimens). ASTM International, West Conshohocken, PA.

ASTM C642-21, 2021. Standard Test Method for Density, Absorption, and Voids in Hardened Concrete. ASTM International, West Conshohocken, PA.

Chang, R., Kim, S., Lee, S., Choi, S., Kim, M., Park, Y., 2017. Calcium carbonate precipitation for CO2 storage and utilization: a review of the carbonate crystallization and polymorphism. Front. Energy Res. 5. doi:10.3389/fenrg.2017.00017.

Cheng, B., Huang, J., Lu, K., Li, J., Gao, G., Wang, T., Chen, H., 2022. BIM-enabled life cycle assessment of concrete formwork waste reduction through prefabrication. Sustain. Energy Technol. Assess. 53, 102449. doi:10.1016/j.seta.2022.102449.

Dixit, A., Du, H., Pang, S.D., 2021. Carbon capture in ultra-high performance concrete using pressurized CO2 curing. Constr. Build. Mater. 288, 123076. doi:10.1016/j.conbuildmat.2021.123076.

Douba, A., Badjatya, P., Kawashima, S., 2022. Enhancing carbonation and strength of MgO cement through 3D printing. Constr. Build. Mater. 328, 126867. doi:10.1016/j.conbuildmat.2022.126867.

Fernández-Carrasco, L., Rius, J., Miravitlles, C., 2008. Supercritical carbonation of calcium aluminate cement. Cem. Concr. Res. 38 (8), 1033–1037. doi:10.1016/j.cemconres.2008.02.013.

Gara, J.A., Zakaria, R., Aminudin, E., Yahya, K., Sam, A.R.M., Loganathan, V.M., Yahya, M.A., Wahi, N., Shamsuddin, S.M., 2022. Effects of the COVID-19 pandemic on construction work progress: an on-site analysis from the sarawak construction project, Malaysia. Sustainability. 14 (10). doi:10.3390/su14106007.

Haghnegahdar, M.R., Rahimi, A., Hatamipour, M.S., 2011. A rate equation for Ca(OH)2 and CO2 reaction in a spouted bed reactor at low gas concentrations. Chem. Eng. Res. Des. 89 (6), 616–620. doi:10.1016/j.cherd.2010.10.019.

He, Z., Li, Z., Shao, Y., 2017. Effect of carbonation mixing on CO2 uptake and strength gain in concrete. J. Mater. Civil Eng. 29 (10), 04017176. doi:10.1061/(ASCE)MT.1943-5533.0002031.

Justnes, H., Skocek, J., Østnor, T.A., Engelsen, C.J., Skjølsvold, O., 2020. Microstructural changes of hydrated cement blended with fly ash upon carbonation. Cem. Concr. Res. 137, 106192. doi:10.1016/j.cemconres.2020.106192.

Kim, M.S., Jun, Y., Lee, C., Oh, J.E., 2013. Use of CaO as an activator for producing a price-competitive non-cement structural binder using ground granulated blast furnace slag. Cem. Concr. Res. 54, 208–214. doi:10.1016/j.cemconres.2013.09.011.

Kim, S., Amr, I.T., Fadhel, B.A., Bamagain, R.A., Hunaidy, A.S., Park, S., Seog, J., Lee, H.K., 2021. The effect of combined carbonation and steam curing on the microstructural evolution and mechanical properties of Portland cement concrete. Adv. Concr. Construct. 11 (5), 367. doi:10.12989/acc.2021.11.5.367.

Liu, P., Chen, Y., Yu, Z., 2020. Effects of temperature, relative humidity and carbon dioxide concentration on concrete carbonation. Mag. Concr. Res. 72 (18), 936–947. doi:10.1680/jmacr.18.00496.

López-Arce, P., Gómez-Villalba, L.S., Martínez-Ramírez, S., Álvarez de Buergo, M., Fort, R., 2011. Influence of relative humidity on the carbonation of calcium hydroxide nanoparticles and the formation of calcium carbonate polymorphs. Powder. Technol. 205 (1), 263–269. doi:10.1016/j.powtec.2010.09.026.

Madadi, A., Wei, J., 2022. Characterization of calcium silicate hydrate gels with different calcium to silica ratios and polymer modifications. Gels. 8 (2). doi:10.3390/gels8020075.

Mehdizadeh, H., Meng, Y., Guo, M.-Z., Ling, T.-C., 2021. Roles of CO2 curing induced calcium carbonates on high temperature properties of dry-mixed cement paste. Constr. Build. Mater. 289, 123193. doi:10.1016/j.conbuildmat.2021.123193.

Mo, L., Panesar, D.K., 2012. Effects of accelerated carbonation on the microstructure of Portland cement pastes containing reactive MgO. Cem. Concr. Res. 42 (6), 769–777. doi:10.1016/j.cemconres.2012.02.017.

Moelich, G.M., Kruger, J., Combrinck, R., 2020. Plastic shrinkage cracking in 3D printed concrete. Compos. Part B, 108313 doi:10.1016/j.compositesb.2020.108313.

Moelich, G.M., Kruger, J., Combrinck, R., 2021. Modelling the interlayer bond strength of 3D printed concrete with surface moisture. Cem. Concr. Res. 150, 106559. doi:10.1016/j.cemconres.2021.106559.

Monkman, S., MacDonald, M., Hooton, R.D., Sandberg, P., 2016. Properties and durability of concrete produced using CO2 as an accelerating admixture. Cem. Concr. Compos. 74, 218–224. doi:10.1016/j.cemconcomp.2016.10.007.

Panda, B., Paul, S.C., Hui, L.J., Tay, Y.W.D., Tan, M.J., 2017. Additive manufacturing of geopolymer for sustainable built environment. J. Clean. Prod. 167, 281–288. doi:10.1016/j.jclepro.2017.08.165.

Qian, X., Wang, J., Fang, Y., Wang, L., 2018. Carbon dioxide as an admixture for better performance of OPC-based concrete. J. CO2 Util. 25, 31–38. doi:10.1016/j.jcou.2018.03.007.

Ravikumar, D., Zhang, D., Keoleian, G., Miller, S., Sick, V., Li, V., 2021. Carbon dioxide utilization in concrete curing or mixing might not produce a net climate benefit. Nat. Commun. 12 (1), 855. doi:10.1038/s41467-021-21148-w.

Rodríguez, N., Alonso, M., Grasa, G., Abanades, J.C., 2008. Process for capturing CO2 arising from the calcination of the CaCO3 used in cement manufacture. Environ. Sci. Technol. 42 (18), 6980–6984. doi:10.1021/es800507c.

Rostami, V., Shao, Y., Boyd, A.J., He, Z., 2012. Microstructure of cement paste subject to early carbonation curing. Cem. Concr. Res. 42 (1), 186–193. doi:10.1016/j.cemconres.2011.09.010.

Shin, Y., Kim, T., Cho, H., Kang, K.-I., 2012. A formwork method selection model based on boosted decision trees in tall building construction. Autom. Constr. 23, 47–54. doi:10.1016/j.autcon.2011.12.007.

Slavcheva, G.S., Feb. 2019. Drying and shrinkage of cement paste for 3D printable concrete. IOP Conf. Ser. 481 (1), 12043. doi:10.1088/1757-899X/481/1/012043.

Sousa, V., Bogas, J.A., 2021. Comparison of energy consumption and carbon emissions from clinker and recycled cement production. J. Clean. Prod. 306, 127277. doi:10.1016/j.jclepro.2021.127277.

Steiner, S., Lothenbach, B., Proske, T., Borgschulte, A., Winnefeld, F., 2020. Effect of relative humidity on the carbonation rate of portlandite, calcium silicate hydrates and ettringite. Cem. Concr. Res. 135, 106116. doi:10.1016/j.cemconres.2020.106116.

Sun, B., Zeng, Q., Wang, D., Zhao, W., 2022. Sustainable 3D printed mortar with CO2 pretreated recycled fine aggregates. Cem. Concr. Compos. 134, 104800. doi:10.1016/j.cemconcomp.2022.104800.

Tay, Y.W.D., Li, M.Y., Tan, M.J., 2019. Effect of printing parameters in 3D concrete printing: printing region and support structures. J. Mater. Process. Technol. 271, 261–270. doi:10.1016/j.jmatprotec.2019.04.007.

Tay, Y.W.D., Lim, S.G., Phua, S.L.B., Tan, M.J., Fadhel, B.A., Amr, I.T., 2023. Exploring carbon sequestration potential through 3D concrete printing. Virt. Phys. Prototyp. 18 (1), e2277347. doi:10.1080/17452759.2023.2277347.

Tu, Z., Guo, M., Poon, C.S., Shi, C., 2016. Effects of limestone powder on CaCO3 precipitation in CO2 cured cement pastes. Cem. Concr. Compos. 72, 9–16. doi:10.1016/j.cemconcomp.2016.05.019.

Villain, G., Thiery, M., Platret, G., 2007. Measurement methods of carbonation profiles in concrete: thermogravimetry, chemical analysis and gammadensimetry. Cem. Concr. Res. 37 (8), 1182–1192. doi:10.1016/j.cemconres.2007.04.015.

Vogler, N., Drabetzki, P., Lindemann, M., Kühne, H.-C., 2022. Description of the concrete carbonation process with adjusted depth-resolved thermogravimetric analysis. J. Therm. Anal. Calorim. 147 (11), 6167–6180. doi:10.1007/s10973-021-10966-1.

Wang, D., Xiao, J., Sun, B., Zhang, S., Poon, C.S., 2023. Mechanical properties of 3D printed mortar cured by CO2. Cem. Concr. Compos. 139, 105009. doi:10.1016/j.cemconcomp.2023.105009.

Xian, X., Shao, Y., 2021. Microstructure of cement paste subject to ambient pressure carbonation curing. Constr. Build. Mater. 296, 123652. doi:10.1016/j.conbuildmat.2021.123652.

Xiao, J., Liu, H., Ding, T., 2021. Finite element analysis on the anisotropic behavior of 3D printed concrete under compression and flexure. Addit. Manuf. 39, 101712. doi:10.1016/j.addma.2020.101712.

Xue, Q., Wang, Z., Chen, Q., 2022. Multi-objective optimization of building design for life cycle cost and CO2 emissions: a case study of a low-energy residential building in a severe cold climate. Build. Simul. 15 (1), 83–98. doi:10.1007/s12273-021-0796-5.

Zaitsev, Y.B., Wittmann, F.H., 1981. Simulation of crack propagation and failure of concrete. Matér. Construct. 14 (5), 357–365. doi:10.1007/BF02478729.

Zajac, M., Skocek, J., Haha, M.Ben, Deja, J., 2022. CO2 mineralization methods in cement and concrete industry. Energies 15 (10). doi:10.3390/en15103597.

Zeyad, A.M., Tayeh, B.A., Adesina, A., de Azevedo, A.R.G., Amin, M., Hadzima-Nyarko, M., Saad Agwa, I., 2022. Review on effect of steam curing on behavior of concrete. Clean. Mater. 3, 100042. doi:10.1016/j.clema.2022.100042.

Zhan, B.J., Poon, C.S., Shi, C.J., 2016. Materials characteristics affecting CO2 curing of concrete blocks containing recycled aggregates. Cem. Concr. Compos. 67, 50–59. doi:10.1016/j.cemconcomp.2015.12.003.